

Journal Pre-proof

Nano CaCO₃ seeding for improving properties of limestone calcined clay cement through in-situ carbonation

Zhonghao Niu, Xiangming Zhou, Pengkun Hou, Mingqing Liu, Shuang Liang, Yuzhou Sun, Yi Zhao, Junjie Wang

PII: S0958-9465(26)00094-6

DOI: <https://doi.org/10.1016/j.cemconcomp.2026.106554>

Reference: CECO 106554

To appear in: *Cement and Concrete Composites*

Received Date: 9 October 2025

Revised Date: 30 January 2026

Accepted Date: 26 February 2026

Please cite this article as: Z. Niu, X. Zhou, P. Hou, M. Liu, S. Liang, Y. Sun, Y. Zhao, J. Wang, Nano CaCO₃ seeding for improving properties of limestone calcined clay cement through in-situ carbonation, *Cement and Concrete Composites*, <https://doi.org/10.1016/j.cemconcomp.2026.106554>.

This is a PDF of an article that has undergone enhancements after acceptance, such as the addition of a cover page and metadata, and formatting for readability. This version will undergo additional copyediting, typesetting and review before it is published in its final form. As such, this version is no longer the Accepted Manuscript, but it is not yet the definitive Version of Record; we are providing this early version to give early visibility of the article. Please note that Elsevier's sharing policy for the Published Journal Article applies to this version, see: <https://www.elsevier.com/about/policies-and-standards/sharing#4-published-journal-article>. Please also note that, during the production process, errors may be discovered which could affect the content, and all legal disclaimers that apply to the journal pertain.

© 2026 Published by Elsevier Ltd.



1 **Nano CaCO₃ seeding for improving properties of limestone calcined clay cement**
2 **through in-situ carbonation**

3 Zhonghao Niu¹, Xiangming Zhou^{1,*}, Pengkun Hou^{2,1,*}, Mingqing Liu¹, Shuang Liang¹, Yuzhou Sun³,
4 Yi Zhao⁴, Junjie Wang⁵

5 ¹ Department of Civil & Environmental Engineering, Brunel University of London, Uxbridge,
6 Middlesex UB8 3PH, United Kingdom

7 ² Shandong Provincial Key Lab for the Preparation & Measurement of Building Materials, School
8 of Materials Science & Engineering, University of Jinan, Jinan 250022, China

9 ³ School of Civil & Transportation Engineering, Henan University of Urban Construction,
10 Pingdingshan 467036, China

11 ⁴ School of Intelligent Construction and Civil Engineering, Zhongyuan University of Technology,
12 Zhengzhou 450007, China

13 ⁵ Department of Civil Engineering, Tsinghua University, Beijing 100084, China

14 * Corresponding author, email: Xiangming.Zhou@brunel.ac.uk; pkhou@163.com

15 **Abstract:**

16 This study proposes an effective strategy to simultaneously enhance the mechanical
17 performance and CO₂ sequestration capacity of limestone calcined clay cement (LC³)
18 incorporating low-grade calcined clay through aqueous carbonation. 25% of the cement
19 fraction in LC³ was subjected to aqueous carbonation for 10 to 40 mins with a water-
20 to-solid ratio of 2.0, leading to the in-situ precipitation of nano-sized CaCO₃. A
21 maximum CO₂ uptake of 15.78% was achieved after 40 min of carbonation. After
22 mixing with the remaining materials of the LC3 formulation, the synergistic dilution
23 and nucleation effects of in-situ nano CaCO₃ promoted the hydration of silicate and
24 aluminate phases, thereby refining the pore structure of LC³. At 3 days, the fraction of
25 fine capillary pores (10-50 nm) increased remarkably, reaching 54% and 60% after 30
26 and 40 min of carbonation, respectively, and this refinement was largely preserved at
27 28 days. Consequently, the 28-day compressive strength of LC³ mortars increased by
28 34.93% and 32.07% at carbonation durations of 30 and 40 min, respectively, compared
29 with the control group. However, substantial consumption of portlandite during pre-
30 carbonation constrained the later development of carboaluminate phases, which
31 highlights a trade-off between enhanced early hydration and limited availability of
32 secondary hydration products. These findings offer new insights into the role of in-situ
33 CaCO₃ precipitation in modifying hydration and pore structure, demonstrating that

34 aqueous carbonation is an effective route to enhance LC³ performance while facilitating
35 CO₂ sequestration.

36 **Keywords:** Aqueous carbonation; CO₂ sequestration; In-situ carbonation; Limestone
37 calcined clay cement; Nano CaCO₃

38 1. Introduction

39 The cement industry is one of the major contributors to global energy consumption and
40 CO₂ emissions, accounting for approximately 6-8% of total anthropogenic CO₂
41 emissions worldwide [1,2]. With the urgent challenges of global climate change, the
42 development of low-carbon and high-performance cementitious materials has become
43 a research priority. Since most CO₂ emissions arise from clinker calcination, reducing
44 clinker content is a widely recognised promising strategy to mitigate the environmental
45 impact of cement production [3].

46 Limestone Calcined Clay Cement (LC³) has attracted increasing attention in recent
47 years due to its reduced clinker factor and favourable mechanical performance [4,5].
48 By partially replacing clinker with calcined clay and limestone, LC³ reduces clinker
49 consumption of approximately 40-50%, resulting in a reduction of CO₂ emissions by
50 about 30-40% per ton of cement, compared with Portland cement [6]. Moreover, the
51 pozzolanic reactivity of calcined clay, combined with the synergistic effect of limestone,
52 promotes the formation of dense hydration products, such as hemicarboaluminate (Hc)
53 and monocarboaluminate (Mc) [7–9], thereby enhancing the mechanical properties and
54 durability of the cementitious matrix. Nevertheless, LC³ suffers from relatively slow
55 early-age hydration and insufficient strength development, which restricts its broader
56 application [10,11].

57 In recent years, various nanoparticles have been explored as hydration accelerators in
58 cement-based materials. Among them, nano-SiO₂ not only provides abundant
59 nucleation sites but also reacts pozzolanically with Ca(OH)₂ to generate additional C-
60 S-H, thereby enhancing later-age strength and structural homogeneity [12–14]. Nano
61 C-S-H seeds serve as precursors or templates for the epitaxial growth of C-S-H, thereby

62 providing the most direct and efficient contribution to hydration kinetics [15,16]. In
63 contrast, nano CaCO_3 promotes hydration through a combined physical-chemical
64 mechanism, since it not only provides filler and nucleation effects but also interacts
65 chemically with reactive aluminates. Moreover, the polymorphs of CaCO_3 (calcite,
66 aragonite, and vaterite) influence the fluidity and compressive strength of cement-based
67 materials due to their differences in solubility and reactivity [17–19].

68 In LC^3 , calcium carbonate plays a crucial role as a major constituent, actively
69 participating in hydration by interacting with alumina phases and stabilising
70 carboaluminate hydrates. While reducing the particle size to the nanoscale can promote
71 these effects by providing additional nucleation sites, the external incorporation of nano
72 CaCO_3 is often limited by agglomeration and poor dispersion, which can limit its
73 efficiency [20,21]. This highlights the necessity for a method that ensures both high
74 intrinsic reactivity and optimal dispersion.

75 To address these dispersion challenges, in-situ aqueous carbonation is proposed.
76 Compared to dry carbonation and semi-dry carbonation, aqueous carbonation exhibits
77 significantly faster reaction kinetics [22], a more uniform carbonation product
78 distribution [23] and relatively simpler process control [24]. Distinct from traditional
79 gas-solid carbonation, the process is primarily controlled by the aqueous diffusion of
80 carbonate species ($\text{CO}_3^{2-}/\text{HCO}_3^-$), generated through the dissolution of CO_2 in the
81 solution. Specifically, calcium-bearing phases (e.g., $\text{Ca}(\text{OH})_2$ and C-S-H) release
82 calcium ions, which then react in situ through a “dissolution-precipitation” process to
83 form nanoscale CaCO_3 and alumina-silica gel, thereby densifying the microstructure
84 [19,25,26]. Notably, the high-water demand of LC^3 is highly compatible with the liquid-
85 rich environment required for aqueous carbonation, ensuring efficient transport. Within
86 the favourable environment, the in-situ generated nanoscale CaCO_3 serves as
87 nucleation sites to promote cement clinker hydration [27]. The carbonated cement
88 slurry, consisting of residues and filtrate obtained after varying carbonation durations,
89 was blended with the other materials of the LC^3 binder. Subsequently, the effects of
90 carbonation duration on fresh properties, mechanical strength, and microstructural
91 development (hydration and pore structure) were analysed. Specifically, the hydration

92 process of LC³ incorporating carbonated cement slurry was investigated using X-ray
 93 diffraction (XRD), thermogravimetric analysis (TG), low-field nuclear magnetic
 94 resonance (LF-NMR), and scanning electron microscopy (SEM).

95 2. Materials and Methods

96 2.1 Materials

97 In this study, commercially available P-I 42.5, produced by Shandong Cement Group,
 98 was used as the main binder. Calcined clay, with a strength activity index of 84.23% in
 99 accordance with ASTM C311 [28], was sourced from Nanjing, China. Calcium
 100 carbonate and gypsum, both supplied by Merck, were used as supplementary materials
 101 for the preparation of LC³. The properties of these materials meet the relevant
 102 requirements specified in ASTM C618 [29].

103 The chemical and mineralogical compositions of the raw materials were determined
 104 using X-ray fluorescence (XRF) and quantitative X-ray powder diffraction (XRD), as
 105 presented in Table 1. The particle size distribution of each raw material is presented in
 106 Fig. 1. Polycarboxylate ether (PCE) superplasticiser was employed to maintain the
 107 comparable flowability of mortars [30,31]

Table 1. Chemical and mineralogical compositions of raw materials
(wt.%)

Oxide	Cement	Calcined clay	Limestone	Gypsum
SiO ₂	18.5	55.95	0.36	0.016
Al ₂ O ₃	3.99	34.62	0.25	0.017
Fe ₂ O ₃	3.40	1.79	0.06	-
CaO	59.17	0.91	54.07	49.48
MgO	3.79	1.75	0.40	0.02
SO ₃	3.41	0.14	0.09	50.44
Na ₂ O	0.23	0.49	-	0.01
K ₂ O	1.18	3.86	0.01	0.01
TiO ₂	0.25	0.28	0.01	-
M _n O	0.09	0.02	-	-
P ₂ O ₅	0.08	0.05	-	-
LOI	1.87	1.07	43.04	20.91
C ₃ S	63.66			
C ₂ S	13.64			
C ₃ A	6.86			

C ₄ AF	8.93
Anhydrite	2.13

108

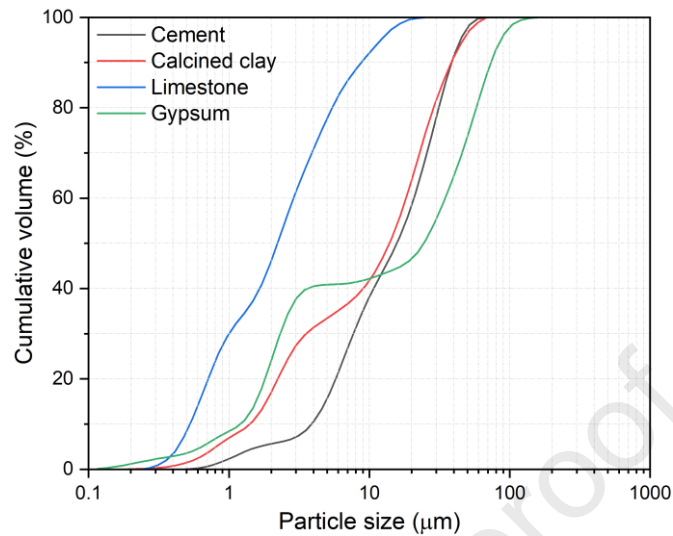


Fig. 1. Particle size distribution of raw materials.

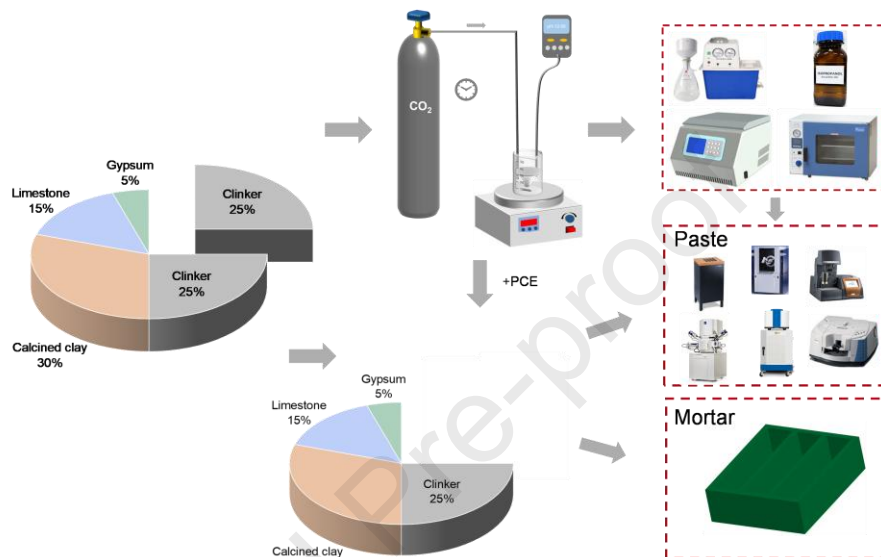
109 2.2 Methodology

110 In this study, the LC³ formulation employed was composed of 50% ordinary Portland
 111 cement, 30% calcined clay, and 15% limestone by mass. Additionally, 5% gypsum
 112 (CaSO₄·2H₂O) was added as a regulator to control the setting behaviour of the binder,
 113 following the procedure established by Avet and Scrivener [7]. The water-to-binder
 114 ratio (w/b) was maintained at a constant value of 0.5 for all mixtures. To investigate the
 115 effect of aqueous carbonation on the hydration and microstructural development of LC³,
 116 25% of the cement was subjected to carbonation by immersion in an aqueous solution
 117 saturated with CO₂, at a water-to-cement ratio of 2.0.

118 2.2.1 Aqueous carbonation of cement suspensions

119 The aqueous carbonation experiments were conducted at ambient temperature and
 120 pressure in a 500 mL beaker containing a cement suspension prepared by mixing 100 g
 121 of cement with 200 g of deionised water. Before carbonation, the suspension was
 122 homogenised by magnetic stirring at 500 rpm for 3 min and maintained at the same
 123 stirring rate throughout the procedure to ensure uniform dispersion. High-purity CO₂
 124 gas (purity > 99.9%) was bubbled into the suspension at a flow rate of 1 L/min through

125 an air stone positioned 1 cm below the liquid surface. The carbonated cement
 126 suspensions were designated CO₂-10, CO₂-20, CO₂-30, and CO₂-40, corresponding to
 127 carbonation durations of 10, 20, 30, and 40 minutes, respectively, with the uncarbonated
 128 suspensions used as the control group (CO₂-0). A schematic of the aqueous carbonation
 129 setup established in this study is presented in Fig. 2.



130
 131 Fig. 2. Schematic view of in-situ carbonation preparation of LC³.
 132

133 After carbonation, the suspension was blended with the remaining raw materials to
 134 prepare LC³ mortars and pastes. To investigate the phase assemblage and
 135 microstructural changes induced by aqueous carbonation, part of the carbonated cement
 136 paste was separated by vacuum filtration, rinsed three times with isopropanol to stop
 137 further hydration and carbonation, and then centrifuged at 3000 rpm for 3 min. The
 138 recovered solids were subsequently vacuum dried at 40 °C for 72h to ensure complete
 139 removal of residual moisture and solvent, according to established procedures [27,32].
 140 The dried samples were then characterised by X-ray diffraction (XRD),
 141 thermogravimetric analysis (TGA), N₂ adsorption-desorption (BET), and scanning
 142 electron microscopy (SEM).

143 2.2.2 Preparation of LC³ mortar and paste

144 The carbonated cement suspension was blended with a polycarboxylate ether (PCE)
 145 superplasticiser and subsequently mixed with the remaining cementitious materials to
 146 ensure uniformity and consistency. Standard sand was added at a sand-to-binder mass
 147 ratio of 3:1, and the mixture was stirred for 5 min in a rotating mixer to produce mortar
 148 specimens. The fresh mortar was cast into $40 \times 40 \times 160$ mm³ prism moulds in
 149 accordance with EN 196-1, compacted by vibration, and covered with plastic film to
 150 minimise moisture loss. Curing was first carried out at 95% relative humidity and $20 \pm$
 151 2 °C for 24h, after which the specimens were demolded and further cured under the
 152 same conditions until testing. The paste and mortar specimens were designated LC³-0,
 153 LC³-10, LC³-20, LC³-30, and LC³-40, corresponding to carbonation durations of 0, 10,
 154 20, 30, and 40 min, respectively, as summarised in Table 1.

Table 2. Mix proportions of LC³ with and without carbonated cement paste

Sample ID	A (%)	B (%)	CO ₂ Duration (min)	Calcined Clay (%)	Limestone (%)	Gypsum (%)	w/b	PCE (%)
LC ³ -0	25	25	0	30	15	5	0.5	0.32
LC ³ -10	25	25	10	30	15	5	0.5	0.51
LC ³ -20	25	25	20	30	15	5	0.5	0.94
LC ³ -30	25	25	30	30	15	5	0.5	1.44
LC ³ -40	25	25	40	30	15	5	0.5	1.86

*A represents the proportion of cement used for in-situ aqueous carbonation

B represents the remaining proportion of cement in LC³

155 2.3 Experimental methods

156 2.3.1 Paste fluidity and setting time

157 After mixing the carbonated cement paste with the remaining constituents of the
 158 mixture for 3 min, the flowability of the LC³ paste was tested using a flow table
 159 according to GB/T 2419-2005 [33]. A truncated cone mould (36 mm × 60 mm × 60 mm)
 160 was filled with the paste and lifted vertically, and the table was operated to complete 25
 161 drops within 25 ± 1 s. The spread diameter was measured in two perpendicular
 162 directions, and their average was taken as the flow value. Each mixture was tested in
 163 triplicate, and the mean result was reported and quoted in the analyses.

164 The setting time of the LC³ paste was measured using a Vicat apparatus in accordance
165 with GB/T 1346-2011 [34]. Fresh paste was placed into the Vicat mould and levelled,
166 and the specimen was kept in a controlled environment at $20 \pm 1^\circ\text{C}$ and relative
167 humidity above 90%. The penetration of the Vicat needle was recorded every 5 minutes.
168 Each mixture was tested in triplicate, and the mean value was reported and quoted in
169 the analyses.

170 2.3.2 Isothermal calorimetry

171 The LC³ paste incorporating carbonated cement paste was homogenised via machine-
172 assisted external mixing for 3 min. Subsequently, a sample of approximately 5.39 g was
173 weighed out. The fresh paste was then immediately transferred into a sealed glass
174 ampoule and placed in a TAM Air (8-channel, Thermometric, USA) isothermal
175 calorimeter. Hydration heat flow and cumulative heat release were continuously
176 recorded for 72h at $25 \pm 0.1^\circ\text{C}$ to assess the early-age hydration kinetics influenced by
177 the in-situ carbonated products. Two independent replicates were conducted to ensure
178 reproducibility.

179 2.3.3 Quantitative X-ray Diffraction (QXRD)

180 Mineralogical identification and quantitative phase analysis of carbonated cement paste
181 and hardened LC³ paste were performed using a Bruker D8 Advance diffractometer
182 (Cu-K α radiation, $\lambda=1.54184 \text{ \AA}$, 40 kV, 40mA). For quantification, 0.8 g of ground
183 paste (passing a 75 μm sieve) was homogenised with 0.2 g of $\alpha\text{-Al}_2\text{O}_3$ as an internal
184 standard (4:1 weight ratio) using ethanol as a dispersant. XRD patterns were recorded
185 over a 2θ range of $5^\circ\text{-}70^\circ$ with a scanning speed of $2^\circ/\text{min}$ and a step size of 0.02° .
186 Phase quantification was performed via Rietveld refinement in TOPAS software. The
187 refinement quality was confirmed by R_p and R_{wp} values below 15%, ensuring the
188 reliability of the resulting phase contents.

189 The corresponding PDF code numbers used for phase identification are provided below:
190 Alite (PDF# 00-042-0551), Belite (PDF# 00-029-0369), Ettringite (PDF# 00-041-

191 1451), Gypsum (PDF# 00-021-0816), Portlandite (PDF# 00-004-0733), Calcite (PDF#
192 00-005-0586), Corundum (PDF# 00-010-0173), Hemi carboaluminate (PDF# 00-041-
193 0221), mono carboaluminate (PDF# 00-041-0219).

194 2.3.4 Scanning electron microscopy (SEM)

195 The morphology of cement particles subjected to different carbonation durations was
196 analysed using a ZEISS Gemini SEM 560 (Zeiss, Germany) equipped with energy-
197 dispersive X-ray spectroscopy (EDS). Before imaging, the samples were rinsed with
198 isopropanol to stop hydration, vacuum-dried at 40 °C for 72h, mounted on aluminium
199 stubs, and sputter-coated with a thin gold layer to improve conductivity.

200 2.3.5 Particle size distribution and specific surface area

201 The particle size distribution of raw materials and carbonated cement particles was
202 measured using a Malvern Mastersizer 2000 (Malvern Instruments, UK). Specific
203 surface area was determined by the BET method, while pore volume and size
204 distribution were calculated using the BJH model from nitrogen adsorption-desorption
205 isotherms (Kubo X1000). Differential pore volume curves from the adsorption branch
206 were used to characterise pore structure.

207 2.3.6 Thermogravimetric analysis (TGA)

208 The hydration of the paste samples was terminated using isopropanol, followed by
209 drying in a vacuum oven at 40 °C for 3 days before TGA. The dried samples were
210 subsequently ground to pass through a 75 µm sieve to ensure homogeneity.
211 Thermogravimetric measurements were performed using a TGA 55 instrument. For
212 each measurement, approximately 7 mg of the prepared powder was heated from 40 °C
213 to 800 °C at a constant heating rate of 10 °C/min. To maintain an inert environment and
214 prevent carbonation, a nitrogen flow of 50 mL/min was continuously applied
215 throughout the heating process.

216 2.3.7 Compressive strength of LC³ mortar

217 The compressive strength of LC³ mortar was measured from 40 mm-side length cubic
218 specimens broken from 40 × 40 × 160 mm³ prismatic samples by flexural bending after
219 curing for 1, 3, 7 and 28 days under a loading rate of 2400 ± 200 N/s, and the average
220 strength obtained from six cubic specimens from the same LC³ formulation was
221 recorded as the corresponding representative strength of the LC³ at each curing age.

222 2.3.8 Low field nuclear magnetic resonance (LF-NMR)

223 Low field nuclear magnetic resonance (LF-NMR) was employed to analyse the pore
224 structure of LC³ paste at 3d, 7d and 28d. For this purpose, a MicroMR20-025V NMR
225 analyser (Niumag, China) operating at 20 MHz was employed to obtain the transverse
226 relaxation time (T₂) distributions. Cylindrical specimens (Φ20mm × 20 mm) were fully
227 saturated for 24h before testing to ensure complete pore filling. All measurements were
228 conducted at 25 ± 1°C, and the average value of three specimens of the same LC³
229 formulation was taken as the corresponding representative value of the mixture for
230 analysis.

231 3 Results and discussion

232 3.1 Characterisation of carbonated cement paste

233 3.1.1 Particle size distribution and specific surface area

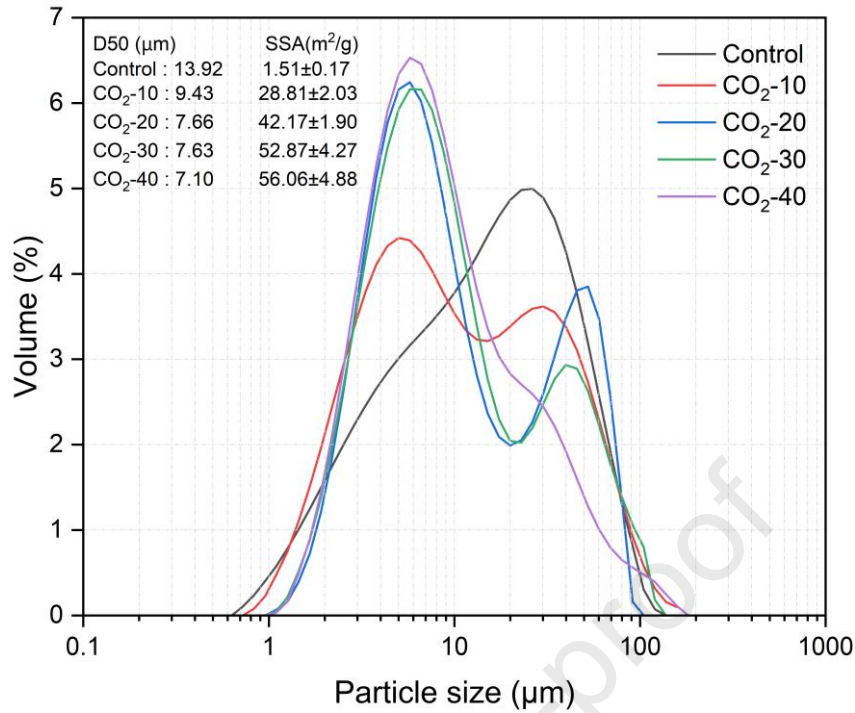


Fig. 3. Particle size distribution of carbonated cement particles.

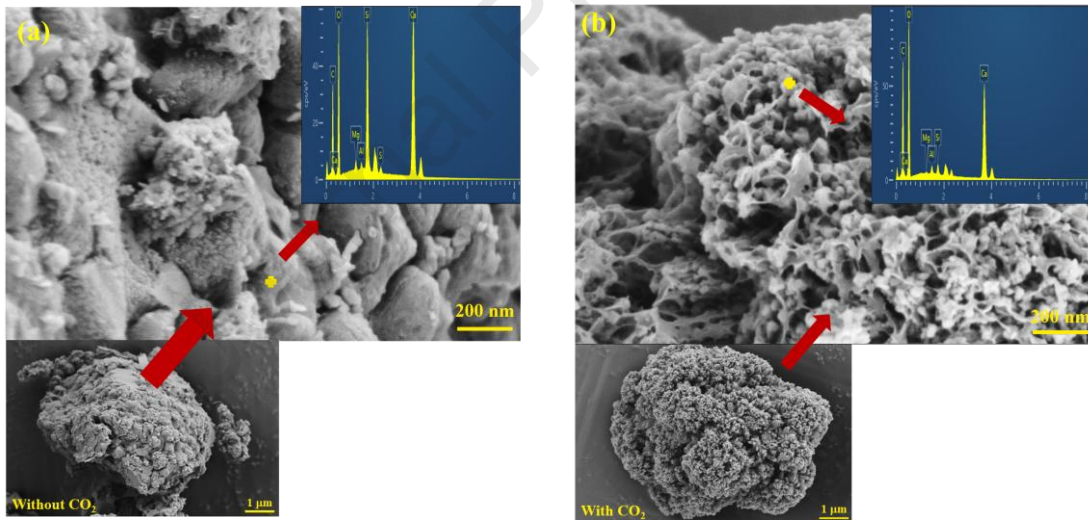


Fig. 4. Cement particles (a) without CO₂ and (b) with CO₂, 30 min.

234 During aqueous carbonation, CO₂ dissolves into the solution to form carbonic acid,
 235 which subsequently dissociates into bicarbonate and carbonate ions under the high-
 236 alkaline environments. Meanwhile, the progressive dissolution of clinker phases,
 237 particularly C₃S, C₂S, and portlandite, reduces the particle size of cement grains and
 238 substantially increases their specific surface area (SSA) (Fig. 3), thereby enhancing ion
 239 exchange and reactivity. The released Ca²⁺ interacts with carbonate species to

240 precipitate CaCO_3 , primarily as amorphous or nano-sized crystallites nucleating on
241 cement particle surfaces. As the carbonation duration increases from 0 to 40 min, the
242 particle size distribution of the carbonated cement powders progressively develops a
243 bimodal pattern, indicating the coexistence of very fine particles and larger
244 agglomerates, which suggests partial flocculation and heterogeneous carbonation of the
245 cement grains. This coupled dissolution-precipitation process also refines the particle
246 morphology (Fig. 4(b)) and increases the density of nucleation sites. SEM-EDS
247 analysis confirms the formation of nanoscale CaCO_3 , and it can be observed that
248 nanoscale CaCO_3 and gel phases are interspersed on the surface of carbonated cement
249 particles.

250 3.1.2 Mineralogical phase

251 As shown in Fig. 5, the XRD patterns reveal that calcite peaks became more distinct
252 with prolonged carbonation and the pH monitoring indicated that all carbonated
253 specimens maintained a high alkalinity, with values remaining above 11.20 throughout
254 the testing period. This high alkalinity, combined with the formation of calcite, indicates
255 the ongoing hydration and carbonation of the calcium silicates (C_3S and C_2S).
256 Meanwhile, the progressive reduction and disappearance of the gypsum peak at 11.62°
257 were observed, suggesting their decomposition and transformation during carbonation.

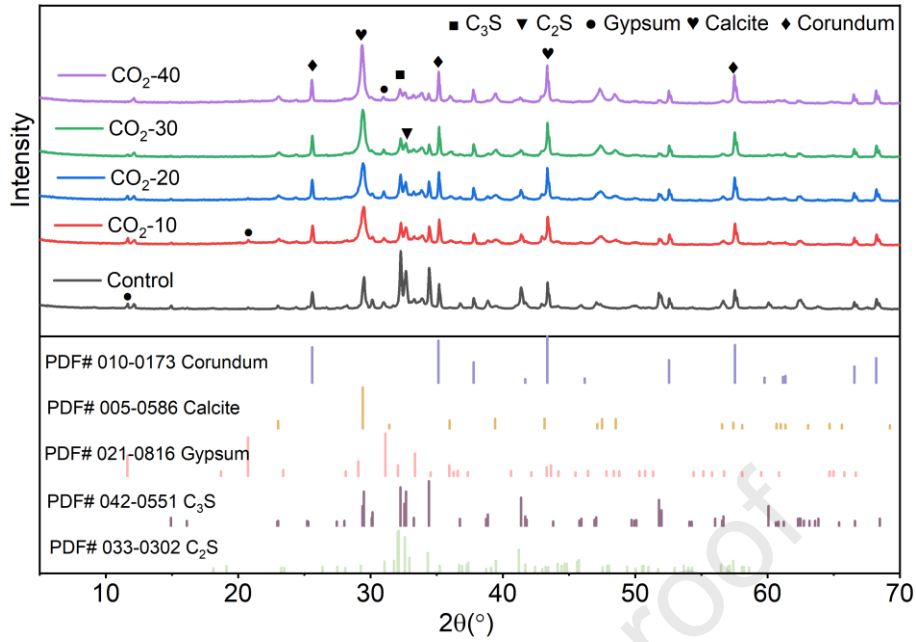


Fig. 5. XRD patterns of carbonated cement particles at different carbonation durations.

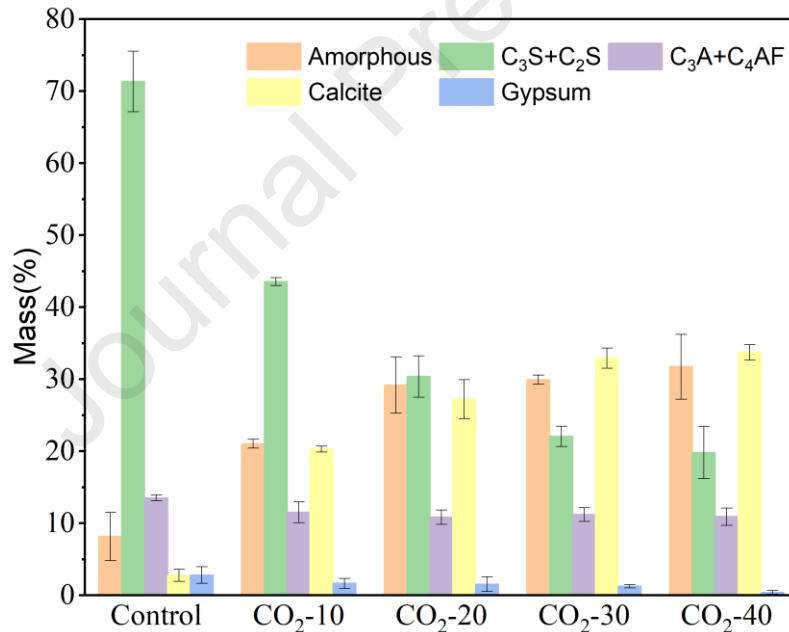


Fig. 6. Mineralogical evolution via QXRD.

258 The quantitative changes in major phases were analysed by Rietveld refinement. As
 259 shown in Fig. 6, the contents of the amorphous phase and calcite varied markedly with
 260 carbonation duration, while the CaCO₃ content remained nearly constant after 30 and
 261 40 min of carbonation. The crystallite size was evaluated by Rietveld refinement based
 262 on the Fundamental Parameter Approach via TOPAS [35], ranging from 36 to 75 nm.
 263 This nanoscale morphology is consistent with the SEM-EDS observations shown in Fig.

264 4, which reveal the formation of nanoscale CaCO₃ particles. The formation of these
 265 nanoscale CaCO₃ is associated with an increase in specific surface area, thereby
 266 providing nucleation sites for continued hydration, as reported by Monkman et al.
 267 [20,36].

268 The formation and content variation of CaCO₃ were further supported by the subsequent
 269 DTG analysis, which quantified the CO₂ uptake and phase evolution during the aqueous
 270 carbonation. As shown in Fig. 7(b), the broad peak in the 40-80 °C range and the sharp
 271 peak at approximately 105 °C are attributed to the dehydration of minor amounts of gel
 272 phases (including C-(A)-S-H and silica gel) and gypsum, respectively. With the
 273 progression of carbonation, C-(A)-S-H was readily decalcified to form CaCO₃ and
 274 silica gel, resulting in an increased intensity of the broad peak at 40-80°C, while the
 275 gypsum peak diminished. Concurrently, the broad peak between 400 and 580 °C,
 276 associated with amorphous CaCO₃ [37], was observed. Furthermore, the sharp peak in
 277 the range of 580-700 °C, corresponding to the decomposition of calcite [38], exhibited
 278 a significant increase in intensity. The progressive increase in peak intensity with
 279 extended carbonation duration reflects the accumulation of stable carbonate phases
 280 within the cement matrix. Fig. 8 compares the CO₂ uptake obtained by the QXRD and
 281 DTG analyses, calculated based on Equations (1) and (2), respectively, in which
 282 m_{CO_2} denotes the molar mass of CO₂, while M_n denotes the mass percentage of the
 283 sample at $n^\circ\text{C}$.

$$284 \quad \text{QXRD: } \text{CO}_2 \text{ uptake (wt. \%)} = M_{\text{CaCO}_3} \times \frac{m_{\text{CO}_2}}{m_{\text{CaCO}_3}} \quad (1)$$

$$285 \quad \text{DTG: } \text{CO}_2 \text{ uptake (wt. \%)} = \frac{M_{400} - M_{700}}{M_{105}} \times 100 \quad (2)$$

286 The results show that the CO₂ uptake determined by DTG is slightly higher due to the
 287 presence of amorphous CaCO₃. Nevertheless, both methods indicate that the CO₂
 288 uptake was in the range of 15-16% after 30 min of carbonation.

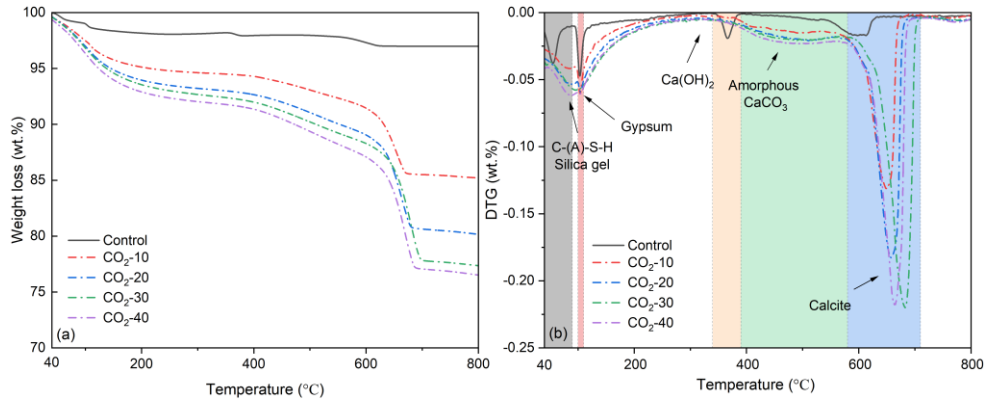


Fig. 7. (a) TG and (b) DTG results of carbonated cement particle.

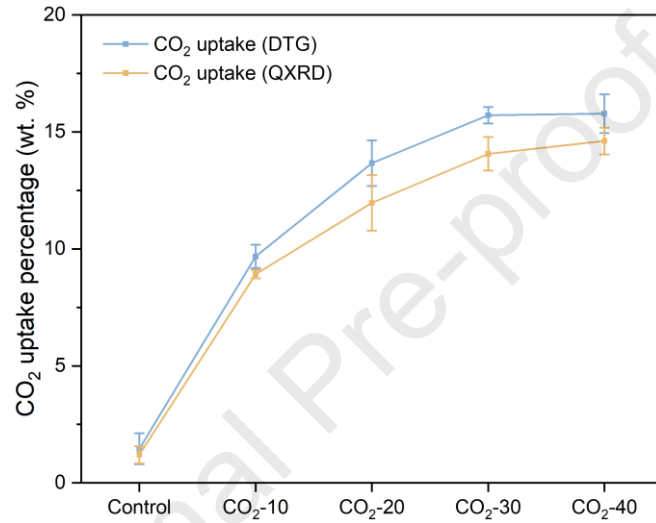


Fig. 8. Comparison of CO₂ uptake calculated by QXRD and DTG

289 3.2 Integration of in-situ carbonation with LC³

290 3.2.1 Fluidity and setting time of LC³ paste

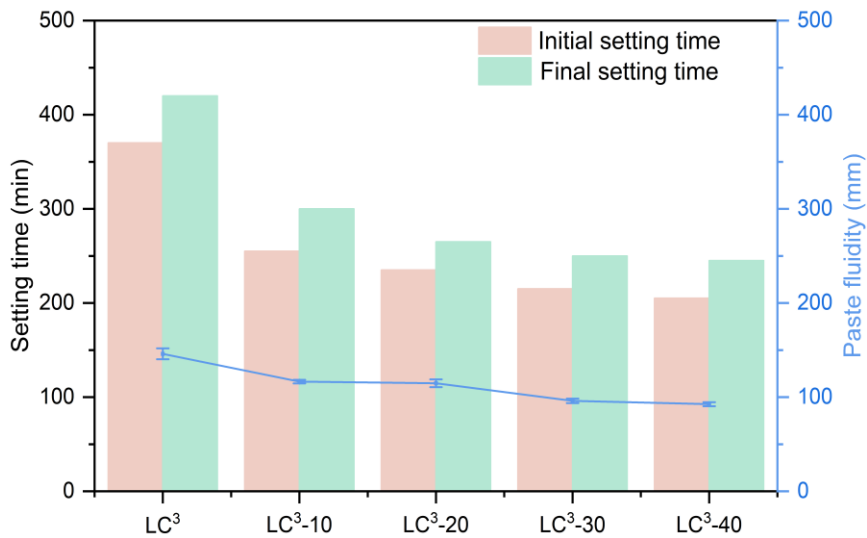
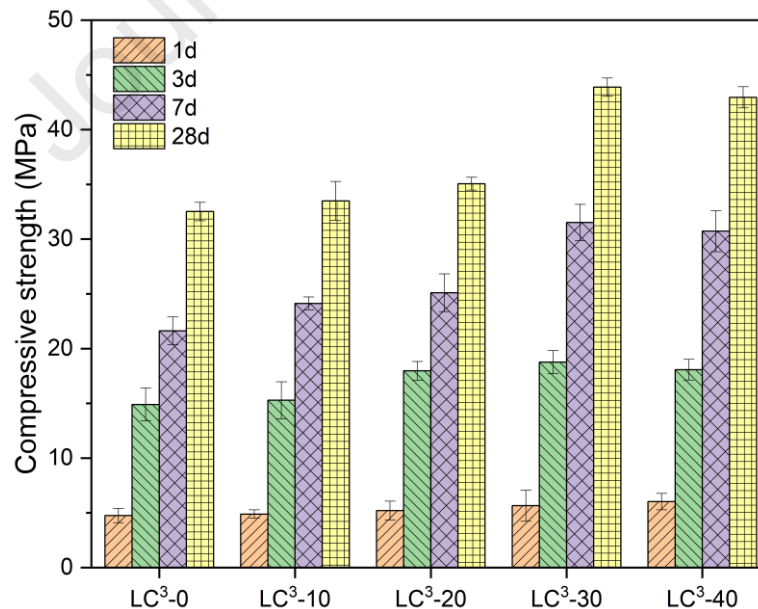


Fig. 9. Setting time and fluidity of LC³ paste with carbonated cement paste

291 As shown in Fig. 9, the calcium carbonate generated during pre-carbonation markedly
 292 reduced both the fluidity and setting time of LC³. Specifically, the initial and final
 293 setting times of LC³-40 decreased by 44.60% and 41.67%, respectively, while the
 294 fluidity of LC³-30 and LC³-40 decreased by 34.25% and 36.64%. These changes can
 295 be primarily attributed to the participation of free water in hydration and carbonation
 296 reactions during pre-carbonation, which promotes the in-situ formation of nano-CaCO₃
 297 and silica gel. The presence of these in-situ nucleated nano-CaCO₃ significantly
 298 accelerates subsequent cement hydration by providing abundant nucleation sites,
 299 thereby shortening the setting time and reducing workability [39]. Moreover, although
 300 carbonation decreases the amount of reactive clinker, the metakaolin fraction remains
 301 unchanged and retains its high specific surface area. Consequently, its strong water
 302 demand and pronounced thickening effect become more dominant, further contributing
 303 to the reduction in fluidity and the acceleration of setting [40].

304 3.2.2 Compressive strength

Fig. 10. Compressive strength of LC³ subject to different carbonation durations.

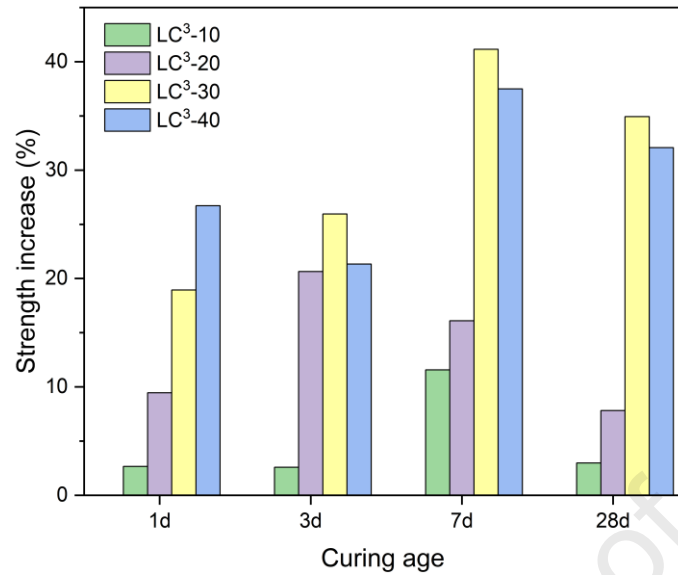


Fig. 11. Compressive strength increasing rates compared to LC³-0 at various ages.

305 The compressive strength results demonstrate that the in-situ formation of CaCO₃
 306 significantly enhanced the compressive strength of LC³ mortar over the curing period.
 307 For LC³-10, short-duration carbonation had a negligible influence, showing values only
 308 comparable to the control group (Fig. 10). With longer carbonation duration, LC³-20,
 309 LC³-30, and LC³-40 exhibited significantly higher strength. At 28d, the compressive
 310 strength of LC³-10, LC³-20, LC³-30, and LC³-40 increased by 2.98%, 7.81%, 34.93%,
 311 and 32.07%, respectively, compared to that of the control group, as shown in Fig. 11.
 312 Despite the relatively low reactivity of the calcined clay used in this study (Reactivity
 313 index of only 84.23%), LC³-30 and LC³-40 achieved compressive strengths of 43.88
 314 and 42.95 MPa, respectively, at 28d, comparable to the EN 197-1 strength class CEM
 315 I 42.5 (28d standard mortar strength \geq 42.5 MPa).

316 Although part of the clinker was consumed during aqueous carbonation to form CaCO₃
 317 and amorphous phases, the carbonated LC³ mortar still exhibited higher compressive
 318 strength than the control group, underscoring the positive role of carbonate products in
 319 hydration. However, further prolongation of the carbonation duration did not lead to
 320 continuous strength development. The slightly lower early-age strength observed in
 321 LC³-40 relative to LC³-30 may be attributed to excessive carbonation, which consumed
 322 reactive clinker phases and produced a dense carbonate layer, thereby hindering
 323 subsequent hydration[41]. In contrast, significant strength gains were observed at later

324 ages. This pronounced late-age strength gain is ascribed to the filler and nucleation
 325 effect of CaCO_3 . Furthermore, the pozzolanic reactivity of silica-rich gel may have also
 326 contributed to this enhancement, as reported by Zajac et al. [42]. These points highlight
 327 the positive contribution of aqueous carbonation to the strength development of LC^3 .

328 3.2.2 Isothermal calorimetry

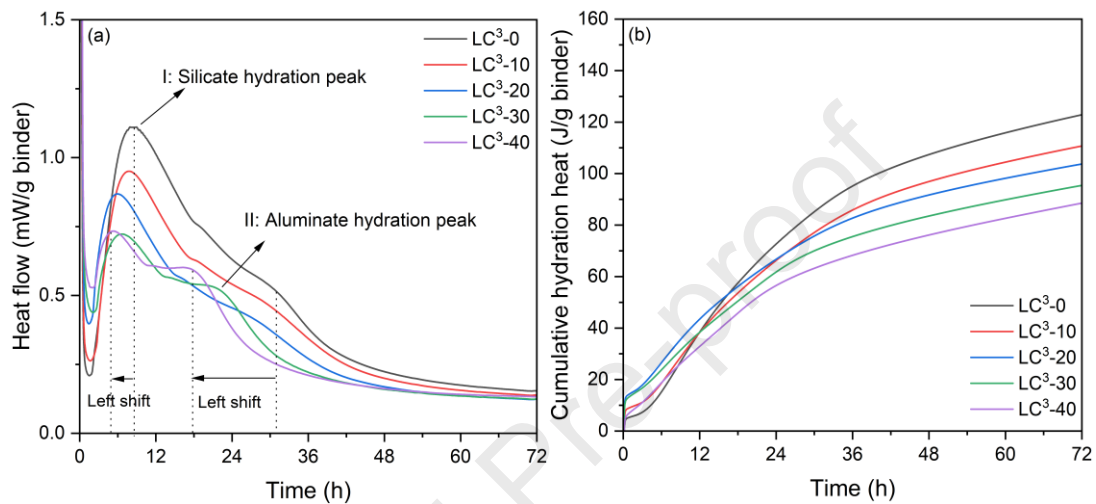


Fig. 12. (a) Hydration heat flow per unit binder mass. (b) Cumulative heat release per unit binder mass

329 Fig. 12 illustrates the heat flow and cumulative hydration heat curves of LC^3 pastes
 330 with and without carbonated cement paste over 72 hours. As shown in Fig. 12(a), the
 331 silicate hydration peak (Peak I) for LC^3 -40 appeared approximately 3.5 h earlier than
 332 that of LC^3 -0, signifying accelerated hydration kinetics. Regarding aluminate hydration
 333 (Peak II), the impact of carbonation was even more pronounced. The onset of LC^3 -40
 334 advanced to 17.6 h, which is nearly 13 hours earlier than that of LC^3 -0, where the
 335 reaction only initiated after 24 h. Similarly, LC^3 -30 also exhibited an onset before 24 h.
 336 These results confirm that CaCO_3 effectively promotes and accelerates the aluminate
 337 hydration process [7].

338 3.2.3 QXRD analysis of LC^3 paste

339

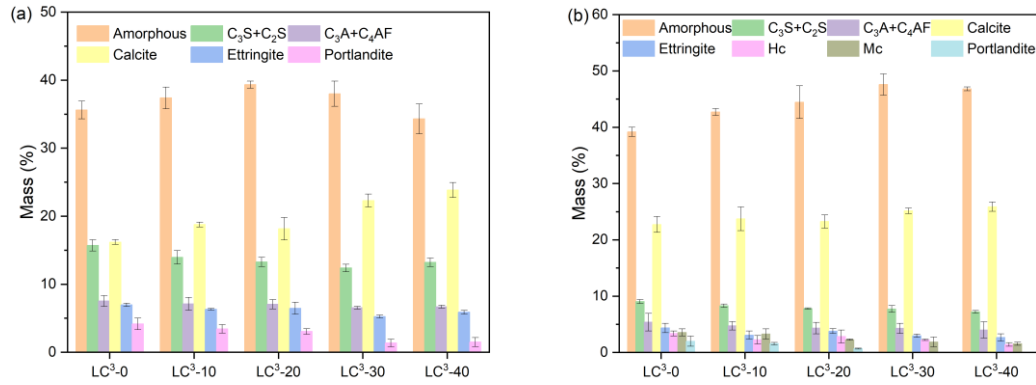


Fig.13. QXRD results of LC³ paste at (a) 1d and (b) 28d.

340 Fig. 13 quantifies the hydration product contents of the samples at 1d and 28d following
 341 duplicate sampling and Rietveld refinement. It reveals distinct differences in CaCO₃
 342 and amorphous phase contents among the samples at 1d (Fig. 13(a)) and further
 343 indicates that extended carbonation results in a marked rise in calcite content with a
 344 concomitant reduction in clinker phase content. Notably, the amorphous phase in LC³-
 345 40 did not show a significant increase compared to that of LC³-0. It appeared slightly
 346 lower than that of LC³-20. However, the compressive strength results indicate that
 347 appropriate carbonation promotes early strength gain, suggesting that the early-age
 348 strength enhancement is not driven by the formation of additional C-S-H gel
 349 (amorphous phase) but primarily by the filler effect of the in-situ formed nanoscale
 350 CaCO₃, which densifies the microstructure.

351 Fig. 13(b) illustrates the quantitative phase assemblage of hydration products at 28d. In
 352 contrast to the results at 1d, the amorphous phase content increased significantly in all
 353 samples, becoming the dominant phase. Specifically, the amorphous content in
 354 carbonated samples (LC³-10 to LC³-40) ranged from 42% to 48%, surpassing that of
 355 the LC³-0, which is around 39%. This substantial growth corresponds to the extensive
 356 formation of C-S-H gel and silica-rich gel derived from the pozzolanic reaction [37].
 357 The 28d QXRD results reveal a marked reduction in Hc and Mc in LC³-30 and LC³-40,
 358 attributed to portlandite depletion, which constrains carboaluminate crystallisation [43].
 359 Nevertheless, the long-term strength development was sustained by the high content of
 360 amorphous gel and residual calcite. The in-situ CaCO₃ served as effective nucleation

361 sites, accelerating the precipitation of hydration products (C-(A)-S-H) and creating a
 362 dense matrix despite the limited presence of carboaluminate.

363 3.2.4 DTG analysis

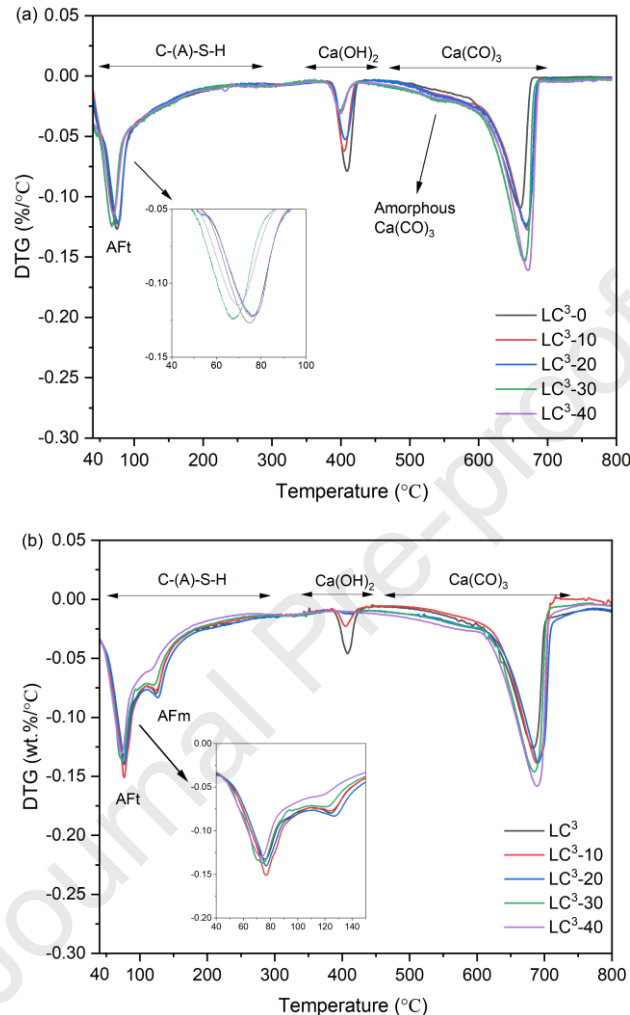


Fig. 14. DTG curve of LC³ paste at (a) 1 d and (b) 28 d.

364 Fig. 14 presents the DTG curves of samples at 1d and 28d, where four distinct peaks
 365 can be identified. The weight loss between 40 °C and 300 °C corresponds to the
 366 dehydration of C-(A)-S-H. The sharp peaks at around 80 °C and 120 °C correspond to
 367 the dehydration of AFt phase (ettringite) and AFm phases (Hc and Mc), respectively.
 368 The peak between 360 °C and 430 °C is associated with the dehydroxylation of calcium
 369 hydroxide, while the weight loss from 430 °C to 600 °C corresponds to the
 370 decomposition of amorphous calcium carbonate (ACC), which is less thermally stable
 371 than crystalline calcite. A strong peak at 600 °C - 700 °C is attributed to decarbonation
 372 of calcite.

373 Thermogravimetric analysis reveals a progressive increase in CaCO_3 content with
 374 longer carbonation durations, accompanied by enhanced compressive strength of early
 375 age, suggesting a positive correlation between carbonation products and mechanical
 376 performance. At 28d, a pronounced reduction in portlandite content was observed in all
 377 samples by DTG and QXRD. This reduction arises from early carbonation of clinker
 378 phases, the pozzolanic reaction of metakaolin, and the formation of Hc and Mc. These
 379 results further demonstrate that early-age pre-carbonation depletes part of the reactive
 380 C_3S and C_2S , which consequently reduces the portlandite produced at later ages. In
 381 $\text{LC}^3\text{-30}$ and $\text{LC}^3\text{-40}$, excessive carbonation caused a pronounced deficiency of
 382 portlandite, thereby constraining AFm formation, whereas in the other groups, the peak
 383 intensity of AFm phases and C-(A)-S-H exhibited significant variation. As shown in
 384 Fig. 15, LC^3 with carbonated cement paste contained more CaCO_3 but less bound water
 385 (40 - 300 °C) compared to the control group. This suggests that the in-situ carbonation
 386 promotes a more uniform distribution of hydration products, which contributes
 387 positively to strength development.

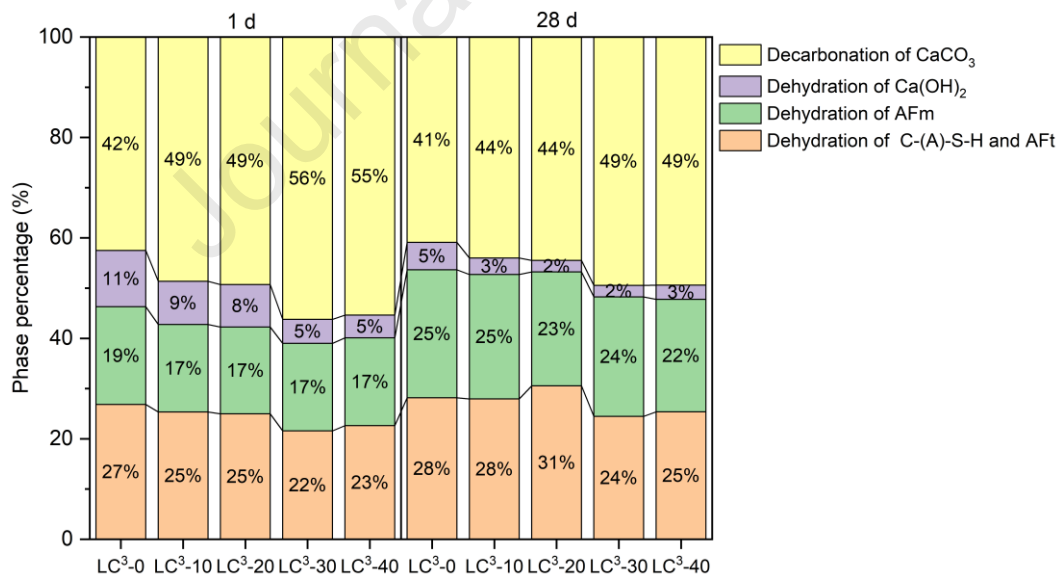


Fig. 15. Mass loss percentage of different hydration products in the samples.

388 3.2.5 Porosity analysis

389 To clarify the role of in-situ CaCO_3 in LC^3 hydration, pore structure analysis was
 390 performed using LF-NMR. Fig. 16 presents the total porosity of all samples at 3d and

391 28d as a function of carbonation duration. Short carbonation times, as in LC³-10 and
 392 LC³-20, resulted in higher porosity than the control group, whereas LC³-30 displayed a
 393 porosity evolution comparable to the control group, suggesting that carbonation for 30
 394 min exerts little influence on pore development. This behaviour can be explained by
 395 the evolution of PSD and SSA during carbonation: initially smooth cement grains
 396 progressively transformed into porous structures (Fig. 4). After 30 min, both D50 and
 397 SSA stabilised, confirming that carbonation duration governs the subsequent hydration
 398 and pore refinement of LC³ paste. For LC³-40, the porosity exhibits an initial increase
 399 followed by a subsequent decrease with hydration time, indicating that a carbonation
 400 duration of 40 min is already approaching an over-carbonation stage. From the SSA
 401 and fluidity results, it can be observed that after 30 minutes of carbonation, the SSA
 402 and fluidity of the cement particles gradually stabilise. At this stage, the silicate phases
 403 within the clinker undergo more pronounced dissolution and decalcification, together
 404 with significant alterations in their microstructural integrity, thereby reducing the
 405 amount of clinker that remains hydraulically active [44]. The progressively reduced
 406 compressive strength of LC³-40 further supports these findings.

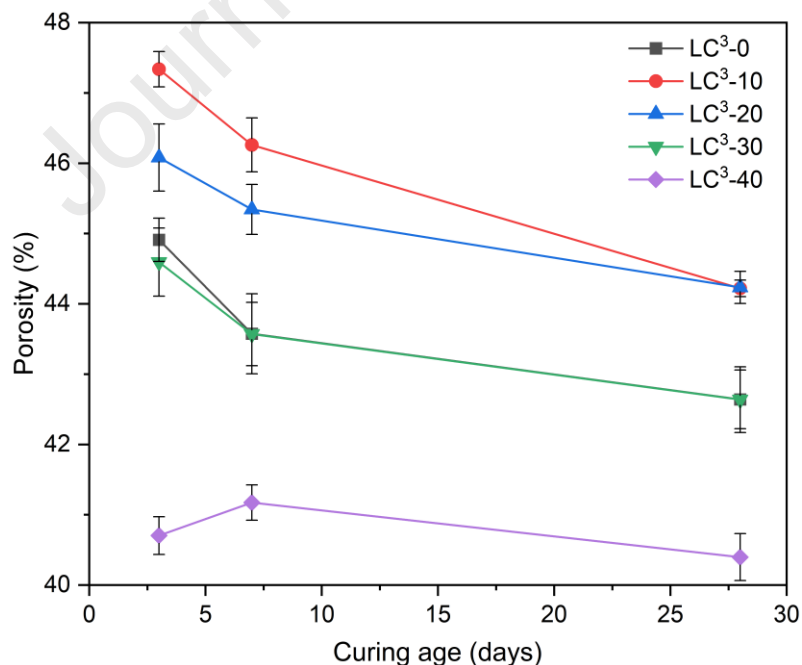


Fig.16. Porosity evolution of LC³ paste at different ages.

407

408 The LF-NMR results further reveal the pore size distribution of samples at 3d and 28d.

409 Pore sizes were classified into four ranges: $d < 10$ nm (gel pores), 10-50 nm (fine
 410 capillary pores), 50 -100 nm (medium capillary pores), and $d > 100$ nm (coarse capillary
 411 pores) [45,46]. Macro-pores (50 nm-1 μ m) are widely recognised as the dominant
 412 factors governing the strength and permeability of cementitious materials [47,48]. In
 413 this study, the pore volume distribution of all samples was mainly concentrated between
 414 10 and 100 nm, indicating a predominantly mesoporous structure with limited macro-
 415 pore development, as shown in Fig. 17.

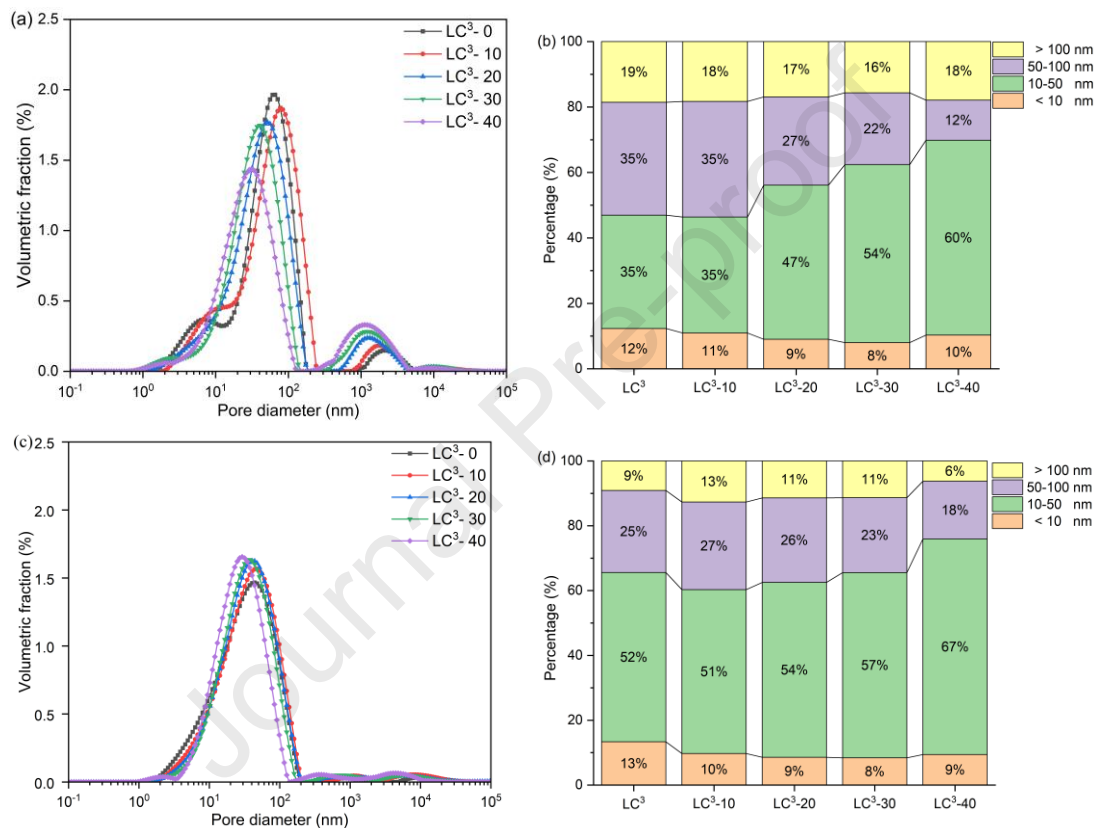


Fig. 17. Pore size distribution of samples at (a) (b) 3d and (c) (d) 28d.

416

417 Figure 17(a) shows the presence of distinct pore size peaks ($d < 10$ nm) in LC³-0 and
 418 LC³-10 at 3d, while the accompanying data in Fig. 17(b) quantifies the shifts in peak
 419 intensity and volume proportion. In contrast, samples subjected to longer carbonation
 420 durations displayed no pronounced peaks in this region, possibly due to the formation
 421 of nano CaCO₃, which promoted the densification of C-(A)-S-H. Compared with the
 422 control group, the primary pore volume distribution peaks of all samples, except LC³-
 423 10, shifted toward smaller pore sizes and exhibited lower intensities, indicating
 424 refinement of gel pores and a reduction in overall gel pore volume. A small fraction of

425 coarse capillary pores (> 100 nm) was also detected in the carbonated samples. This
 426 may be attributed to the local dissolution of cement particles during aqueous
 427 carbonation and subsequent precipitation of nano CaCO_3 , which can leave larger voids
 428 at original sites.

429 By 28d, the proportion of coarse capillary pores disappeared, as shown in Fig. 17(c).
 430 Meanwhile, the peak intensity of all samples incorporating carbonated cement paste
 431 was higher than that of the control, and the peak positions exhibited a progressive shift
 432 toward smaller pore sizes with increasing carbonation duration. A reduction in the
 433 proportion of pores > 100 nm was identified, accompanied by an increase in fine
 434 capillary pores (10-50 nm), as shown in Fig. 17(d), the in-situ carbonation promoted
 435 the in-situ formation of calcium carbonate particles on the cement surface, which
 436 facilitated the further hydration of LC^3 cement clinker, thereby densifying its
 437 microstructure and improving its strength. The refinement effect was also particularly
 438 evident at 3d, with the fraction of fine capillary pores increased by 2.49%, 36.00%,
 439 57.04%, and 71.95% for carbonation durations of 10, 20, 30, and 40 min, respectively.
 440 Although this refined distribution weakened over time, the proportion of fine capillary
 441 pores remained higher at 28d than that of the control. Such pore refinement, induced by
 442 CaCO_3 and amorphous phases, is expected to contribute positively to the strength
 443 development of LC^3 , as shown in Fig. 18.

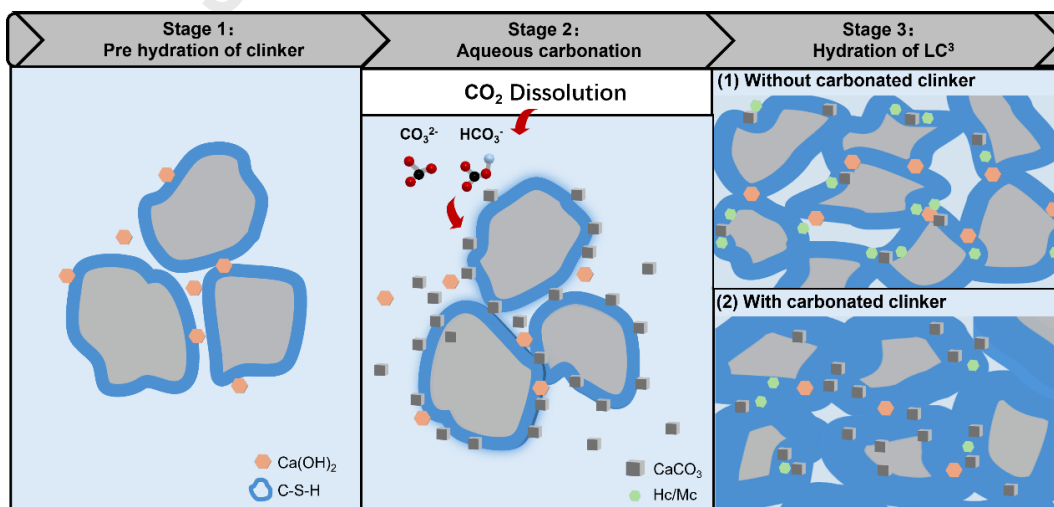


Fig. 18. Schematic diagrams of in-situ CaCO_3 formation and its impact on LC^3

445 Conclusion

446 This study demonstrates that partial pre-carbonation of the LC³ cement fraction
447 produces in-situ nano sized CaCO₃ that reshapes early hydration, microstructure
448 development, and mechanical performance through nucleation and dilution effects.
449 First, in situ CaCO₃ supplies abundant nucleation sites that advance both the silicate
450 (Peak I) and aluminate (Peak II) hydration events, increasing early cumulative heat on
451 a binder basis. Afterwards, this nucleation advantage translates into rapid refinement
452 within the mesopore band (10-50 nm), as evidenced by the leftward shift and
453 intensification of PSD peaks and the elevation of the fine-capillary fraction to 28d.
454 Moreover, the same pre-carbonation converts part of the reactive clinker into carbonate,
455 progressively depleting portlandite and moderating the extent of carboaluminate (i.e.
456 Hc and Mc) formation at later ages. Consequently, nucleation-driven densification
457 surpasses clinker dilution within an optimal dosage, achieving pronounced strength
458 gains. Considering both the process and property, 30 minutes of carbonation (CO₂
459 uptake \approx 15%) was believed to be an optimum. LC³-30 and LC³-40 mortars exhibit
460 about 30% higher 28d strength than the control group, approaching the EN 197-1 CEM
461 I 42.5 strength class, despite the relatively modest reactivity of the calcined clay used.
462 Nevertheless, at later ages, strength development is controlled by microstructural
463 densification, indicating that the nucleation/filler roles of in situ CaCO₃ effectively
464 compensate dilution up to a threshold. Based on the experimental results and analyses,
465 the main conclusions can be drawn:

- 466 1) Aqueous carbonation led to the in-situ formation of nanoscale CaCO₃, which is
467 interspersed with gel phase and adheres to the surface of cement particles. The
468 increased specific surface area of the cement provided additional nucleation sites,
469 effectively accelerating the hydration kinetics of silicate and aluminate phases in
470 LC³. However, the progressive consumption of portlandite during pre-carbonation
471 restricted the later formation of hemicarboaluminate and monocarboaluminate,
472 highlighting a trade-off between enhanced early hydration and limited availability
473 of secondary hydration products.
- 474 2) In-situ generated nano CaCO₃ significantly improved the compressive strength of

475 LC³ mortar. At 28d, the strength of LC³-30 and LC³-40 increased by 34.93% and
476 32.7%, respectively, compared with the control, with 30 min identified as the
477 optimum carbonation duration, corresponding to a CO₂ uptake of 15.71%.

478 3) The presence of in-situ formed nano-CaCO₃ refined the pore structure of LC³,
479 particularly within the 10-50 nm range. The proportion of fine capillary pores
480 increased markedly at early ages and remained higher than the control at 28d,
481 corresponding to long-term strength development.

482 From a sustainability perspective, the approach established in this study couples clinker
483 reduction intrinsic to LC³ with measurable CO₂ uptake during aqueous carbonation.
484 The observed maximum uptake and the concurrent strength enhancement indicate a
485 pathway to lower embodied CO₂ per unit performance. Practically, aqueous carbonation
486 offers a controllable route to dispense nanoscale CaCO₃ without the dispersion
487 challenge commonly associated with ex-situ nano-additions, mitigating agglomeration
488 and improving spatial uniformity of nucleation sites. However, further investigation of
489 long-term durability is needed, as the reduction in portlandite content resulting from in-
490 situ carbonation limits AFm formation, which may influence durability that depends on
491 Ca(OH)₂ and AFm (e.g., sulfate attack and chloride attack).

492

493 **Acknowledgement**

494 The authors would like to thank the financial support from the UKRI under grant
495 EP/X04145X/1 (i.e., the CSTO2NE project), the European Commission under grant
496 893469 (i.e. the NEASCMs project), the Royal Society under grant IEC\NSFC\223146,
497 the Major Innovation Project of Guangxi Zhuang Autonomous Region (Grant No.
498 2024AA10004), and the China-Africa Joint Laboratory for Advanced Low-Carbon
499 Cementitious Materials (Grant No. 2023YFE0126000). The first author would also like
500 to thank Zhongyuan University of Technology for providing a partial PhD scholarship
501 to him to proceed with this study at Brunel University of London

502 **Reference**

- 503 [1] F. Zunino, K. Scrivener, The reaction between metakaolin and limestone and its
504 effect in porosity refinement and mechanical properties, *Cem. Concr. Res.* 140
505 (2021) 106307. <https://doi.org/10.1016/j.cemconres.2020.106307>.
- 506 [2] T. Jiang, K. Cui, J. Chang, Development of low-carbon cement: Carbonation of
507 compounded C2S by β -C2S and γ -C2S, *Cem. Concr. Compos.* 139 (2023)
508 105071. <https://doi.org/10.1016/j.cemconcomp.2023.105071>.
- 509 [3] B. Lothenbach, K. Scrivener, R.D. Hooton, Supplementary cementitious
510 materials, *Cem. Concr. Res.* 41 (2011) 1244–1256.
511 <https://doi.org/10.1016/j.cemconres.2010.12.001>.
- 512 [4] G.E. Abdelaziz, H. Shoukry, A.A. Selim, M.S. Saif, Recent Progress in
513 Limestone-Calcined Clay Cement (LC3): A Review, in: *Materials Science*
514 *Forum*, Trans Tech Publications Ltd, 2023: pp. 165–174.
515 <https://doi.org/10.4028/p-74p7so>.
- 516 [5] K. Scrivener, F. Martirena, S. Bishnoi, S. Maity, Calcined clay limestone cements
517 (LC3), *Cem. Concr. Res.* 114 (2018) 49–56.
518 <https://doi.org/10.1016/j.cemconres.2017.08.017>.
- 519 [6] K. Hosen, B. Chen, Limestone calcined clay cement (LC3): A review of
520 materials, properties, production and environmental impact, *J.Build. Eng.* 112
521 (2025) 113672. <https://doi.org/10.1016/j.job.2025.113672>.
- 522 [7] F. Avet, K. Scrivener, Investigation of the calcined kaolinite content on the
523 hydration of Limestone Calcined Clay Cement (LC3), *Cem. Concr. Res.* 107
524 (2018) 124–135. <https://doi.org/10.1016/j.cemconres.2018.02.016>.
- 525 [8] Y. Zhao, Y. Zheng, J. He, K. Cui, P. Shen, C.S. Poon, G. Peng, R. Guo, D. Xia,
526 Development of reactive carbonate-calcined clay-cement (C4) composites
527 through synchronizing aluminate-carbonate reaction: Toward high compressive
528 strength and low carbon emission, *Cem. Concr. Compos.* 160 (2025).
529 <https://doi.org/10.1016/j.cemconcomp.2025.106060>.
- 530 [9] X. Qian, J. Wang, L. Wang, Y. Fang, Enhancing the performance of metakaolin
531 blended cement mortar through in-situ production of nano to sub-micro calcium
532 carbonate particles, *Construct. Build. Mater.* 196 (2019) 681–691.
533 <https://doi.org/10.1016/j.conbuildmat.2018.11.134>.
- 534 [10] B. Liu, X. Gu, H. Wang, J. Liu, M.L. Nehdi, Y. Zhang, Study on the mechanism
535 of early strength strengthening and hydration of LC3 raised by shell powder,
536 *J.Build. Eng.* 98 (2024). <https://doi.org/10.1016/j.job.2024.111422>.
- 537 [11] Y. Yu, M. Yang, C. Wan, L. Lin, Mechanical, workability, economic and
538 environmental properties of concrete with limestone calcined clay cement and
539 recycled aggregates, *Sci. Rep.* 15 (2025). <https://doi.org/10.1038/s41598-025-97539-6>.
- 540
541 [12] M. Liu, X. Zhou, P. Hou, R. Hai, Y. Sun, S. Liang, Z. Niu, Effects of colloidal
542 nanoSiO₂ on the hydration and hardening properties of limestone calcined clay
543 cement (LC3), *Construct. Build. Mater.* 411 (2024) 134371.
544 <https://doi.org/10.1016/j.conbuildmat.2023.134371>.

- 545 [13] R.S. Lin, S. Oh, W. Du, X.Y. Wang, Strengthening the performance of limestone-
546 calcined clay cement (LC3) using nano silica, *Construct. Build. Mater.* 340
547 (2022). <https://doi.org/10.1016/j.conbuildmat.2022.127723>.
- 548 [14] K. Khan, W. Ahmad, M.N. Amin, S. Nazar, Nano-Silica-Modified Concrete: A
549 Bibliographic Analysis and Comprehensive Review of Material Properties,
550 *Nanomaterials* 12 (2022) 1989. <https://doi.org/10.3390/nano12121989>.
- 551 [15] X. Li, J. Dengler, C. Hesse, Reducing clinker factor in limestone calcined clay-
552 slag cement using C-S-H seeding – A way towards sustainable binder, *Cem.*
553 *Concr. Res.* 168 (2023) 107151.
554 <https://doi.org/10.1016/j.cemconres.2023.107151>.
- 555 [16] E. Berodier, K. Scrivener, Understanding the filler effect on the nucleation and
556 growth of C-S-H, *J. Am. Ceram. Soc.* 97 (2014) 3764–3773.
557 <https://doi.org/10.1111/jace.13177>.
- 558 [17] D. Zhao, J.M. Williams, A.H.A. Park, S. Kawashima, Rheology of cement pastes
559 with calcium carbonate polymorphs, *Cem. Concr. Res.* 172 (2023) 107214.
560 <https://doi.org/10.1016/j.cemconres.2023.107214>.
- 561 [18] D. Zhao, J.M. Williams, Z. Li, A.H.A. Park, A. Radlińska, P. Hou, S. Kawashima,
562 Hydration of cement pastes with calcium carbonate polymorphs, *Cem. Concr.*
563 *Res.* 173 (2023) 107270. <https://doi.org/10.1016/j.cemconres.2023.107270>.
- 564 [19] Y. Zhou, F. Wu, L. Jinag, B. Lu, G. Hou, J. Zhu, Production of vaterite via wet
565 carbonation of carbide residue: Enhancing cement properties and CO₂
566 sequestration, *Cem. Concr. Compos.* 150 (2024) 105549.
567 <https://doi.org/10.1016/j.cemconcomp.2024.105549>.
- 568 [20] S. Monkman, Y. Sargam, L. Raki, Comparing the effects of in-situ nano-calcite
569 development and ex-situ nano-calcite addition on cement hydration, *Construct.*
570 *Build. Mater.* 321 (2022) 126369.
571 <https://doi.org/10.1016/j.conbuildmat.2022.126369>.
- 572 [21] V.T. Nguyen, S.Y. Lee, D.J. Kim, Simulation of the effect of nano-CaCO₃
573 agglomeration on the hydration process and microstructural evolution of cement
574 paste, *Case Stud. Constr. Mater.* 19 (2023) e02612.
575 <https://doi.org/10.1016/j.cscm.2023.E02612>.
- 576 [22] Y. Jiang, L. Peng, Z. Ma, J. xin Lu, P. Shen, C.S. Poon, Enhancing the treatment
577 efficiency of recycled concrete fines with aqueous carbonation, *Cem. Concr. Res.*
578 174 (2023). <https://doi.org/10.1016/j.cemconres.2023.107338>.
- 579 [23] Z. Liu, J. Du, W. Meng, Achieving low-carbon cementitious materials with high
580 mechanical properties using CaCO₃ suspension produced by CO₂ sequestration,
581 *J. Clean. Prod.* 373 (2022). <https://doi.org/10.1016/j.jclepro.2022.133546>.
- 582 [24] M. Zajac, J. Skibsted, P. Durdzinski, F. Bullerjahn, J. Skocek, M. Ben Haha,
583 Kinetics of enforced carbonation of cement paste, *Cem. Concr. Res.* 131 (2020)
584 106013. <https://doi.org/10.1016/j.cemconres.2020.106013>.
- 585 [25] M. Zajac, I. Maruyama, A. Iizuka, J. Skibsted, Enforced carbonation of
586 cementitious materials, *Cem. Concr. Res.* 174 (2023) 107285.
587 <https://doi.org/10.1016/j.cemconres.2023.107285>.
- 588 [26] Z. Ma, Y. Jiang, J. He, P. Shen, Q. Qin, Z. Gu, J. Li, C.S. Poon, Revealing the

- 589 connection between carbonation regimes and early pozzolanic reactivity of
590 recycled concrete powder: Impact of composition and microstructure, *Cem.*
591 *Concr. Res.* 186 (2024). <https://doi.org/10.1016/j.cemconres.2024.107697>.
- 592 [27] S. Luo, M. Wang, B.T. Pham, N. De Belie, T.C. Ling, Performance evaluation of
593 mixing carbonated reactive magnesia slurry in Portland cement pastes, *Cem.*
594 *Concr. Compos.* 160 (2025).
595 <https://doi.org/10.1016/j.cemconcomp.2025.106065>.
- 596 [28] ASTM C311/C311M-18, Standard Test Methods for Sampling and Testing Fly
597 Ash or Natural Pozzolans for Use in Portland-cement Concrete, ASTM
598 International, West Conshohocken, PA, (2018).
- 599 [29] ASTM C618, Standard specification for coal fly ash and raw or calcined natural
600 pozzolan for use in concrete, (2015).
- 601 [30] L. Liu, Y. Ji, F. Gao, L. Zhang, Z. Zhang, X.Y. Liu, Study on high-efficiency
602 CO₂ absorption by fresh cement paste, *Constr. Build. Mater.* 270 (2021).
603 <https://doi.org/10.1016/j.conbuildmat.2020.121364>.
- 604 [31] Z. Zhao, T. Qi, W. Zhou, D. Hui, C. Xiao, J. Qi, Z. Zheng, Z. Zhao, A review on
605 the properties, reinforcing effects, and commercialization of nanomaterials for
606 cement-based materials, *Nanotechnol. Rev.* 9 (2020) 349–368.
607 <https://doi.org/10.1515/ntrev-2020-0023>.
- 608 [32] S. Monkman, Y. Sargam, O. Naboka, B. Lothenbach, Early age impacts of CO₂
609 activation on the tricalcium silicate and cement systems, *J. CO₂ Util.* 65 (2022)
610 102254. <https://doi.org/10.1016/j.jcou.2022.102254>.
- 611 [33] GBT 2419-2005, GB/T 2419, Method for Determination of Fluidity of Cement
612 Mortar, Chinese Standards Association, China, 2005.
- 613 [34] GB/T 1346, Test Methods for Water Requirement of Normal Consistency,
614 Setting Time and Soundness of the Portland Cement, Chinese Standards
615 Association, China, 2011.
- 616 [35] S. Krishnan, S.K. Kanaujia, S. Mithia, S. Bishnoi, Hydration kinetics and
617 mechanisms of carbonates from stone wastes in ternary blends with calcined clay,
618 *Constr. Build. Mater.* 164 (2018) 265–274.
619 <https://doi.org/10.1016/J.CONBUILDMAT.2017.12.240>.
- 620 [36] S. Monkman, B.E.J. Lee, K. Grandfield, M. MacDonald, L. Raki, The impacts
621 of in-situ carbonate seeding on the early hydration of tricalcium silicate, *Cem.*
622 *Concr. Res.* 136 (2020) 106179.
623 <https://doi.org/10.1016/j.cemconres.2020.106179>.
- 624 [37] M. Zajac, J. Skibsted, F. Bullerjahn, J. Skocek, Semi-dry carbonation of recycled
625 concrete paste, *J. CO₂ Util.* 63 (2022) 102111.
626 <https://doi.org/10.1016/j.jcou.2022.102111>.
- 627 [38] Z. Yu, Y. Meng, K.H. Mo, H. Liu, T.C. Ling, Influences of w/c and CO₂ curing
628 duration on the high temperature properties of cement pastes, *J. Build. Eng.* 69
629 (2023) 106293. <https://doi.org/10.1016/j.jobe.2023.106293>.
- 630 [39] Q. Fu, Z. Zhang, X. Zhao, W. Xu, D. Niu, Effect of nano calcium carbonate on
631 hydration characteristics and microstructure of cement-based materials: A review,
632 *J. Build. Eng.* 50 (2022). <https://doi.org/10.1016/j.jobe.2022.104220>.

- 633 [40] F. Nazário Santos, S. Raquel Gomes de Sousa, A. José Faria Bombard, S. Lopes
634 Vieira, Rheological study of cement paste with metakaolin and/or limestone
635 filler using Mixture Design of Experiments, *Construct. Build. Mater.* 143 (2017)
636 92–103. <https://doi.org/10.1016/j.conbuildmat.2017.03.001>.
- 637 [41] N. Saeki, L. Cheng, R. Kurihara, T. Ohkubo, A. Teramoto, Y. Suda, R. Kitagaki,
638 I. Maruyama, Natural carbonation process in cement paste particles in different
639 relative humidities, *Cem. Concr. Compos.* (2023) 105400.
640 <https://doi.org/10.1016/j.cemconcomp.2023.105400>.
- 641 [42] J. Song, M. Zajac, M. Ben Haha, J. Skibsted, Impact of Ca/Si and Al/Si ratios on
642 the composition and structure of the alumina-silica gel formed by wet
643 carbonation of synthesized C-S-H in blends with portlandite and ettringite, *Cem.*
644 *Concr. Res.* 197 (2025). <https://doi.org/10.1016/j.cemconres.2025.107931>.
- 645 [43] F. Zunino, E. Zurich, J. Sun, K. Scrivener, Challenges and opportunities of LC3
646 with less than 50% clinker, n.d.
647 <https://www.researchgate.net/publication/374255810>.
- 648 [44] Y. Jiang, L. Li, J. xin Lu, P. Shen, T.C. Ling, C.S. Poon, Mechanism of
649 carbonating recycled concrete fines in aqueous environment: The particle size
650 effect, *Cem. Concr. Compos.* 133 (2022).
651 <https://doi.org/10.1016/j.cemconcomp.2022.104655>.
- 652 [45] B. Song, S. Liu, X. Hu, K. Ouyang, G. Li, C. Shi, Compressive strength, water
653 and chloride transport properties of early CO₂-cured Portland cement-fly ash-
654 slag ternary mortars, *Cem. Concr. Compos.* 134 (2022) 104786.
655 <https://doi.org/10.1016/j.cemconcomp.2022.104786>.
- 656 [46] Z. Yang, C. Zhou, Pore Structure of Water-Saturated Cement Mortars by Low-
657 Field Nuclear Magnetic Resonance, *Journal of the Chinese Ceramic Society* 50
658 (2022) 1391–1400. <https://doi.org/10.14062/j.issn.0454-5648.20210660>.
- 659 [47] X. Chen, S. Wu, J. Zhou, Experimental study and analytical model for pore
660 structure of hydrated cement paste, *Appl. Clay Sci.* 101 (2014) 159–167.
661 <https://doi.org/10.1016/j.clay.2014.07.031>.
- 662 [48] J. Zhu, R. Zhang, Y. Zhang, F. He, The fractal characteristics of pore size
663 distribution in cement-based materials and its effect on gas permeability, *Sci.*
664 *Rep.* 9 (2019). <https://doi.org/10.1038/s41598-019-53828-5>.

Declaration of interests

The authors declare that they have no known competing financial interests or personal relationships that could have appeared to influence the work reported in this paper.

The authors declare the following financial interests/personal relationships which may be considered as potential competing interests:

Journal Pre-proof